Geophysical Research Letters

RESEARCH LETTER
10.1029/2018GL081756

Detecting Regional Modes of Variability in Observation-Based Surface Ocean pCO_2

Peter Landschützer[1], **Tatiana Ilyina**[1], **and Nicole S. Lovenduski**[2]

[1]Max Planck Institute for Meteorology, Hamburg, Germany, [2]Department of Atmospheric and Oceanic Sciences and Institute of Arctic and Alpine Research, University of Colorado, Boulder, CO, USA

Key Points:
- Frequency of observation-based pCO_2 variability corresponds to frequencies in AMO, PDO, MEI, and SAM index
- The majority of the ocean variability is driven by circulation/biology, whereas the North Atlantic signal is temperature driven
- Decadal pCO_2 signals emerge in all basins; their detection is limited by the short observational record

Correspondence to:
P. Landschützer,
peter.landschuetzer@mpimet.mpg.de

Citation:
Landschützer, P., Ilyina, T., & Lovenduski, N. S. (2019). Detecting regional modes of variability in observation-based surface ocean pCO_2. *Geophysical Research Letters*, *46*, 2670–2679. https://doi.org/10.1029/2018GL081756

Received 19 DEC 2018
Accepted 26 FEB 2019
Accepted article online 4 MAR 2019
Published online 7 MAR 2019

Abstract We use a neural network-based estimate of the sea surface partial pressure of CO_2 (pCO_2) derived from measurements assembled within the Surface Ocean CO_2 Atlas to investigate the dominant modes of pCO_2 variability from 1982 through 2015. Our analysis shows that detrended and deseasonalized sea surface pCO_2 varies substantially by region and the respective frequencies match those from the major modes of climate variability (Atlantic Multidecadal Oscillation, Pacific Decadal Oscillation, multivariate ENSO index, Southern Annular Mode), suggesting a climate modulated air-sea exchange of CO_2. We find that most of the regional pCO_2 variability is driven by changes in the ocean circulation and/or changes in biology, whereas the North Atlantic variability is tightly linked to temperature variations in the surface ocean and the resulting changes in solubility. Despite the 34-year time series, our analysis reveals that we can currently only detect one to two periods of slow frequency oscillations, challenging our ability to robustly link pCO_2 variations to climate variability.

Plain Language Summary In our study we show that there is a link between the amount of carbon in the surface ocean and natural climate variability. We find that this variability is very different between different oceanic regions, but most of the observed variability is on decadal timescales and longer. Current data products therefore do not extend long enough in time to robustly detect long-term oscillations of the surface ocean carbon content.

1. Introduction

The global oceans absorb roughly 25% of the annually emitted carbon dioxide (CO_2) by human activities and thereby play a substantial role in moderating the effects of climate change (Le Quéré et al., 2018). While historically marine carbon budgets were largely based on ocean carbon cycle models (e.g., Aumont & Bopp, 2006; Assmann et al., 2010; Buitenhuis et al., 2010; Doney et al., 2009; Galbraith et al., 2010; Graven et al., 2012; Ilyina et al., 2013; Matear & Lenton, 2008), in recent years a series of observation-based estimates of the air-sea CO_2 exchange have emerged (Rödenbeck et al., 2015), challenging our understanding of the air-sea flux variability on interannual to decadal timescales (Landschützer et al., 2015; Ritter et al., 2017; Rödenbeck et al., 2015). These estimates rely upon surface ocean CO_2 measurements gathered within the two largest databases, namely the Lamont-Doherty Earth Observatory (Takahashi et al., 2018) and the Surface Ocean CO_2 Atlas (SOCAT) databases (Bakker et al., 2016). The databases contain the to-date largest collections of measurements of the surface ocean partial pressure of CO_2 (pCO_2) and the CO_2 fugacity, that is, the pCO_2 equivalent corrected for the nonideal behavior of the gas. To estimate the exchange of CO_2 between the atmosphere and the ocean from these data bases, the surface measurements are extrapolated using various novel approaches from statistical techniques based on autocorrelation (S. D. Jones et al., 2015) to machine learning approaches such as neural networks (Landschützer et al., 2013; Nakaoka et al., 2013; Zeng et al., 2014).

The new observation-based estimates suggest substantial variations in the global ocean carbon sink, especially on decadal timescales (Landschützer et al., 2016; Rödenbeck et al., 2015). Particularly noteworthy are the Tropical Pacific variability (Rödenbeck et al., 2015) and the decadal variability in Southern Ocean CO_2 flux (DeVries et al., 2017; Gregor et al., 2018; Gruber et al., 2019; Landschützer et al., 2015; Ritter et al., 2017), that is, the least observed ocean basin responsible for the majority of the oceanic uptake and storage of anthropogenic carbon (Frölicher et al., 2015; Gruber et al., 2009; Khatiwala et al., 2013). Substantial CO_2

flux variability has also been noted in the North Pacific and other ocean basins (Landschützer et al., 2016; Rödenbeck et al., 2015).

Despite the advancements in data-interpolation techniques as well as the increasing abundance of measurements, observation-based estimates of the air-sea CO_2 exchange still rely heavily on data extrapolation, causing substantial differences between estimates (Ritter et al., 2017; Rödenbeck et al., 2015). Furthermore, the majority of available measurements and auxiliary driver data is only available for the recent past (Bakker et al., 2016), limiting the time period the CO_2 flux can be estimated with a certain degree of confidence. Previously, regional studies have linked the air-sea flux variability to atmospheric dynamics in the Tropical Pacific (Feely et al., 2006), the North Atlantic (Breeden & McKinley, 2016; Schuster & Watson, 2007), the Tropical Atlantic (Lefèvre et al., 2016), and the Southern Ocean (Le Quéré et al., 2007; Lovenduski et al., 2007). However, an attempt to attribute the dominant mode of variability on global scale to one single climate mode using empirical orthogonal function analysis has failed to identify a clear connection (Landschützer et al., 2016). Understanding the modes of local and global pCO_2 variability as well as identifying their origin is essential to understand the contemporary marine carbon cycle, but also provides the basis for near term predictions and future projections (Li et al., 2016; Lovenduski et al., 2019; Séférian et al., 2018).

Here, we use a neural network-based estimate (Landschützer et al., 2013) of the sea surface pCO_2 derived from shipboard measurements from 1982 through 2015 to investigate the spatial and temporal structure of sea surface pCO_2 anomaly, that is, the primary driver of air-sea CO_2 flux anomalies. We investigate for each major ocean basin the dominant frequency of pCO_2 variability and show that they compare well with the spectral structure of the major climate modes on the basin-scale, but vary substantially when resolved for refined $1° \times 1°$ regions.

2. Methods

Our analysis is based on the 2-step self-organizing map feed-forward (SOM-FFN) approach by Landschützer et al. (2013) in its global configuration (Landschützer et al., 2014). In a first step the global ocean is divided into provinces of similar surface carbon content using a neural network-based clustering approach, that is, a self-organizing map. Within these highly dynamic provinces the actual partial pressure of CO_2 is then reconstructed using a nonlinear neural network regression approach (feed-forward network) where auxiliary driver data known to drive the surface ocean carbonate system are regressed against available gridded observations from the fourth release of the SOCAT (Bakker et al., 2016; Sabine et al., 2013). The method reproduces annual available observations (from SOCAT as well as independent observations from time series and data from the Lamont Doherty Earth Observatotory database that are not included in SOCAT) nearly bias free (see Landschützer et al., 2016) and has further been shown to accurately reproduce the observed variability in the SOCAT observations (Rödenbeck et al., 2015). While observational coverage varies in time, with fewer observations in the 1980s and 1990s, the reconstructed pCO_2 shows no temporal bias increasing confidence in the reconstruction of temporal signals. More details regarding the method as well as its extensive validation can be found in Landschützer et al. (2016) and Landschützer et al. (2018).

We focus our analysis both on the grid scale as well as on larger biogeochemical provinces from a combination of the Fay and McKinley (2014) biomes. In order to reduce the number of biomes we combine some of the smaller scale biomes within each basin, namely, we combine the subtropical permanently stratified biome, the subpolar seasonally stratified biome and subtropical seasonally stratified biome. In the South Atlantic we combine the equatorial biome and the subtropical permanently stratified biome, whereas we separate the Southern Ocean by combining the subtropical seasonally stratified and subpolar seasonally stratified biomes. We exclude the marginal sea ice biome (ICE) to avoid direct biogeochemistry-sea ice interactions—see Figure 1. In this way, we roughly divide the global ocean into six regions: (a) the Pacific Ocean except the tropical regions, (b) the Tropical Pacific Ocean, (c) the Indian Ocean, (d) the North Atlantic, (e) the South Atlantic, and (f) the Southern Ocean. Choosing this large-scale basin structure washes out some of the smaller dynamical features of each basin, but it has the advantage that our variability results may be directly linked to the climate modes known to drive the variability in these basins.

In order to isolate the dominant interannual signals within our pCO_2 time series, we first remove a linear least-squares fit to the data and focus on the resulting anomalies. We further remove the seasonal cycle using a 12-month average filter as the seasonal cycle dominates most of the variability globally. The remaining anomaly time series, we convert from time into frequency space using a fast-fourier transformation. In order

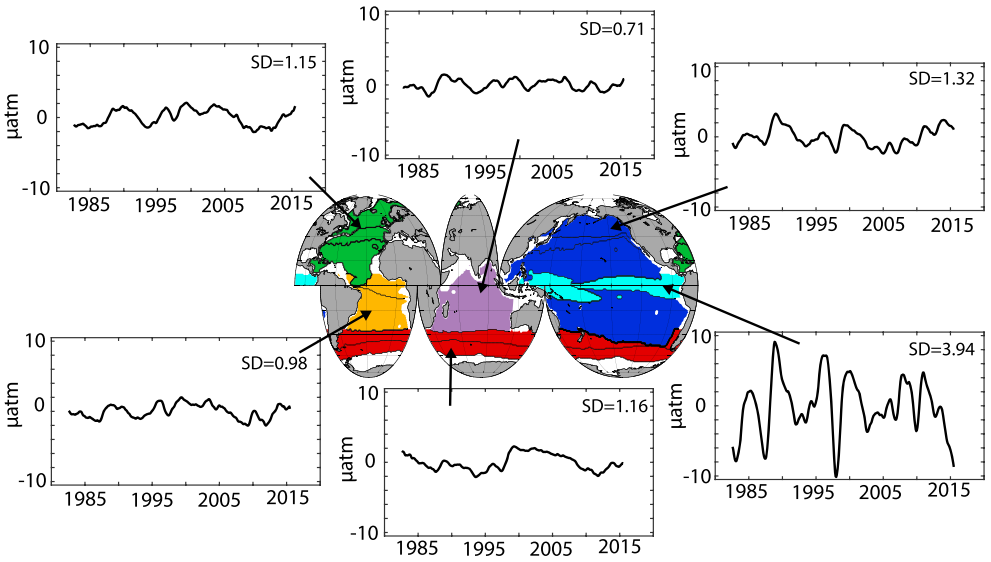

Figure 1. Sea surface pCO_2 anomaly time series for six large-scale ocean regions defined by combining the time mean Fay and McKinley biomes (indicated by black lines in the center map). The regions include the North Atlantic, the South Atlantic, the Indian Ocean, the Pacific Ocean excluding the tropics, the Tropical Pacific, and the Southern Ocean. Numbers in the top-right corners refer to the standard deviation (SD) of the respective anomaly time series. Colors on the map indicate the regions and arrows direct to the anomaly time series.

to link the observed anomalies to processes either related to temperature or circulation/biology, we use the temperature sensitivity of CO_2 of $\gamma_T = 4.23\%$ per degree Celsius proposed by Takahashi et al. (1993). While local sensitivities might divert from this experimentally determined number we assume this to have only a small impact on our results. Following Takahashi et al. (2002) we can perturb the long-term mean pCO_2, $<pCO_2>$, with the observed temperature anomalies to derive the thermally driven changes in time:

$$pCO_2^{th} =< pCO_2 > \cdot \exp(\gamma_T \cdot (\mathrm{SST} - < \mathrm{SST} >)). \quad (1)$$

Furthermore, we can extract the nonthermal counterpart by removing the temperature effect from the pCO_2 time series.

$$pCO_2^{nt} = pCO_2 \cdot \exp(\gamma_T \cdot (< \mathrm{SST} > - \mathrm{SST})). \quad (2)$$

We compare the observed fluctuations with index data from commonly used climate indices, that is, the Pacific Decadal Oscillation (PDO, Zhang et al., 1997), the multivariate ENSO index (MEI, Wolter & Timlin, 2011), the Atlantic Multidecadal Oscillation (AMO, Enfield et al., 2001), and the Southern Annular Mode (SAM, Marshall, 2003). The MEI represents the first principal component of six observed variables over the Tropical Pacific Ocean, namely, sea level pressure, u and v surface wind components, sea surface temperature, surface air temperature, and total cloudiness fraction (Wolter, 1987), and represents the environmental response to the El Niño Southern Oscillation climate phenomenon usually oscillating between its positive (El Niño) and its negative (La Niña) phase on 3- to 7-year timescales (Feely et al., 1999, 2006). During positive MEI phases (i.e., El Niño), the equatorial trade winds weaken resulting in reduced equatorial upwelling of subsurface water masses and likewise an increase in surface water temperatures (see, e.g., Feely et al., 2006). The PDO represents an extension of the ENSO-like pattern (Deser et al., 2012) across the entire Pacific Ocean basin but includes also a dominant signal at decadal timescales. Its index is calculated from the first principal component of the sea surface temperature in the North Pacific Ocean (Zhang et al., 1997), where positive PDO phases correspond to negative temperature anomalies. The AMO describes significant fluctuations in the sea surface temperature on multidecadal timescales of the North Atlantic and has been shown previously by model studies to drive large-scale changes in the sea surface pCO_2 (see, e.g., Breeden & McKinley, 2016). Positive AMO phases are associated with increasing surface temperatures and a significant reduction in surface ocean DIC in the North Atlantic Ocean (Breeden & McKinley, 2016). Finally, the

SAM index describes the zonal pressure difference between 40 and 65°S and positive SAM phases correspond with increasing strength of westerly winds (Marshall, 2003). This strengthening of the westerlies in turn leads to increased upwelling of carbon rich subsurface waters leading to an increase in the sea surface pCO_2 (Le Quéré et al., 2007; Lovenduski et al., 2007; Xue et al., 2018).

All these indices represent large-scale climate variability which we detrend and deseasonalize in the same way as the pCO_2 time series. The choice of indices follows our choice of our large-scale regions and the exclusion of the at least partly ice-covered regions. Therefore, we do not discuss other climatic links that have been suggested in the past to influence the local and high latitude pCO_2 variability such as the Arctic Oscillation and North Atlantic Oscillation (see, e.g., Landschützer et al., 2016; McKinley et al., 2004; Schuster & Watson, 2007; Thomas et al., 2008).

3. Results and Discussions

The observation-based SOM-FFN pCO_2 shows strong anomalies in the regional time series (Figure 1). In the tropical band of the Pacific Ocean the strongest magnitude of variability can be observed ranging from −10 to 10 μatm around the mean annual pCO_2. The variability in all remaining biomes is of similar magnitude but does not exceed ±2.5 μatm. Likewise, the standard deviation of the Tropical Pacific anomaly exceeds those of the other basins. This highlights that overall the Tropical Pacific variability is fout times larger than the variability observed in all other basins in agreement with a model study by Le Quéré et al. (2000). Due to the large area of the chosen biomes, however, their smaller fluctuations compared to the Tropical Pacific in the sea surface pCO_2 can have a large impact on the global air-sea CO_2 flux (Landschützer et al., 2015). While at first glance the intrabasin anomalies are rather different, the two Atlantic Ocean biome anomalies reveal a strong correspondence, indicating the possibility of these fluctuations being connected. The Southern Ocean variability suggests little connection with the other biomes, as it is nearly devoid of high frequency variability.

Figure 2 further illustrates the anomalies in frequency space. Here we plot the inverse of the frequency, that is, the phase, for better visualization of the observed oscillations. In the Tropical Pacific and Indian Ocean (Figure 2a), that is, those regions where previous studies observed connections to changes in tropical trade winds (e.g., Feely et al., 2006; Fay & McKinley, 2013; Rödenbeck et al., 2014; Valsala et al., 2010), we find the shortest oscillation cycles in the range of a few years up to 8 years. The cycles up to 5 years correspond well with the peaks in the phase diagram of the PDO and the MEI over the same time period. The Pacific Ocean anomaly reveals moderate negative correlations with the PDO and the MEI ($R = -0.35$ and -0.57, respectively). We further find a tighter link between the anomalies in the Tropical Pacific biomes with the PDO and MEI index anomalies ($R = -0.54$ and -0.86, respectively), due to the equatorial origin of the ENSO driven oscillation cycles and the tight link between ENSO and PDO (Deser et al., 2012). Correlating the pCO_2 anomaly power spectrum with the power spectra of the indices, however, reveals a stronger link ($R = 0.74$ and 0.80, respectively, for the Pacific Ocean and $R = 0.64$ and 0.95, respectively, for the Tropical Pacific).

In the North Pacific the observed variability is tightly linked to the North Pacific PDO dipole pattern. The western part of the basin experiences stronger mixing and cooling resulting in a stronger upward transport of inorganic carbon (Fay & McKinley, 2013; Ishii et al., 2014; Landschützer et al., 2016). This is also evident in Figure 3a, where the relative thermal and nonthermal pCO_2 contributions for the respective frequencies are displayed. Here, the circulation-/biology-driven pCO_2 component dominates at frequencies corresponding to those from the total pCO_2 variability and the PDO but also the MEI at time intervals of 3, 5, and 8 years, respectively. An increase in the MEI index represents a slowdown of the vertical transport of dissolved inorganic carbon along the equator and along the North American coastline (Feely et al., 2006; Ishii et al., 2014; Rödenbeck et al., 2014), which is counteracted by warmer surface waters and a thermally driven increase in pCO_2. Overall these compensating mechanisms lead to a decrease of the surface pCO_2 with an increasing MEI index (Fay & McKinley, 2013; Feely et al., 1999, 2006; McKinley et al., 2004). This is again evident in Figure 3b where the nonthermal component of the pCO_2 variability dominates the respective frequencies identified as peaks in the frequency diagram of the Tropical Pacific and MEI (Figure 2a). The Indian Ocean is connected and impacted by the Pacific Ocean variability through the Indonesian Through Flow (Sarma et al., 2013; Valsala et al., 2010). The decomposition into drivers (Figure 3c), however, reveals that despite the strong correspondence between thermal and nonthermal components and the MEI index spectra (Figure 2), both components nearly cancel each other out resulting in very limited net pCO_2 variations

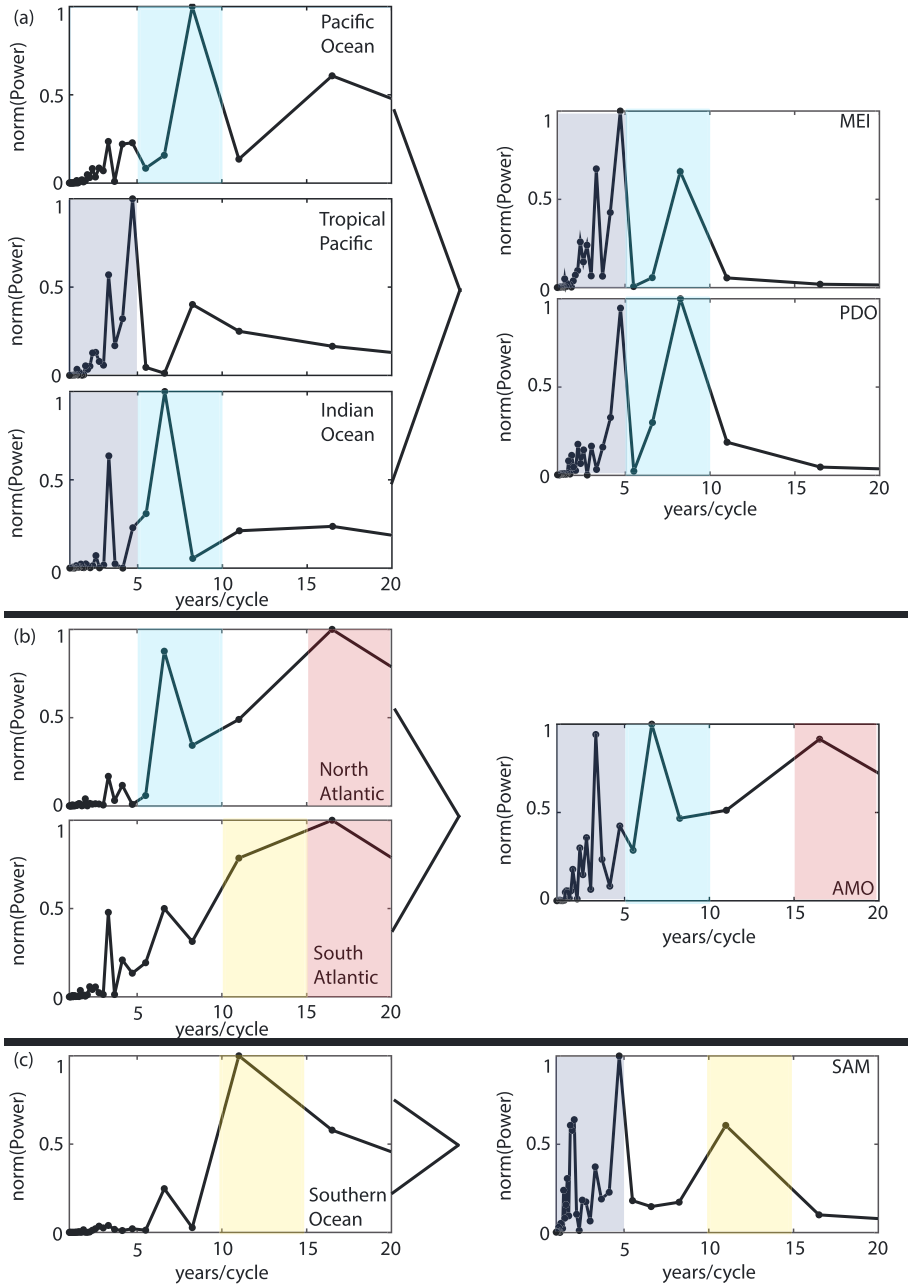

Figure 2. Normalized sea surface pCO_2 anomalies in frequency space in comparison with the frequency diagrams of the major climate modes linked to the respective regions. (a) shows the Pacific Ocean excluding the tropics, the Tropical Pacific, and the Indian Ocean in comparison to the PDO and MEI indices; (b) shows the North and South Atlantic in comparison to the AMO; and (c) shows the Southern Ocean in comparison with the SAM index. Colored areas highlight 5-year intervals where peaks in the frequency diagram occur. PDO = Pacific Decadal Oscillation; MEI = Multivariate ENSO Index; AMO = Atlantic Multidecadal Oscillation; SAM = Southern Annular Mode.

in the Indian Ocean. The largest fluctuations observed in the Indian Ocean are in the order of 7 years, entirely driven by temperature variations.

Continuing our analysis in the Atlantic Ocean (Figure 2b) shows that both North and South Atlantic basin variability is dominated by the low frequency pCO_2 variability. Additionally, strong oscillations at 7-year intervals in the North and 12-year intervals in the South Atlantic occur. At first sight this corresponds to the low frequency peak in the AMO spectrum. While the direct correlation between the AMO anomalies and the North and South Atlantic pCO_2 anomalies reveals only a moderate connection ($R = 0.31$ and 0.32,

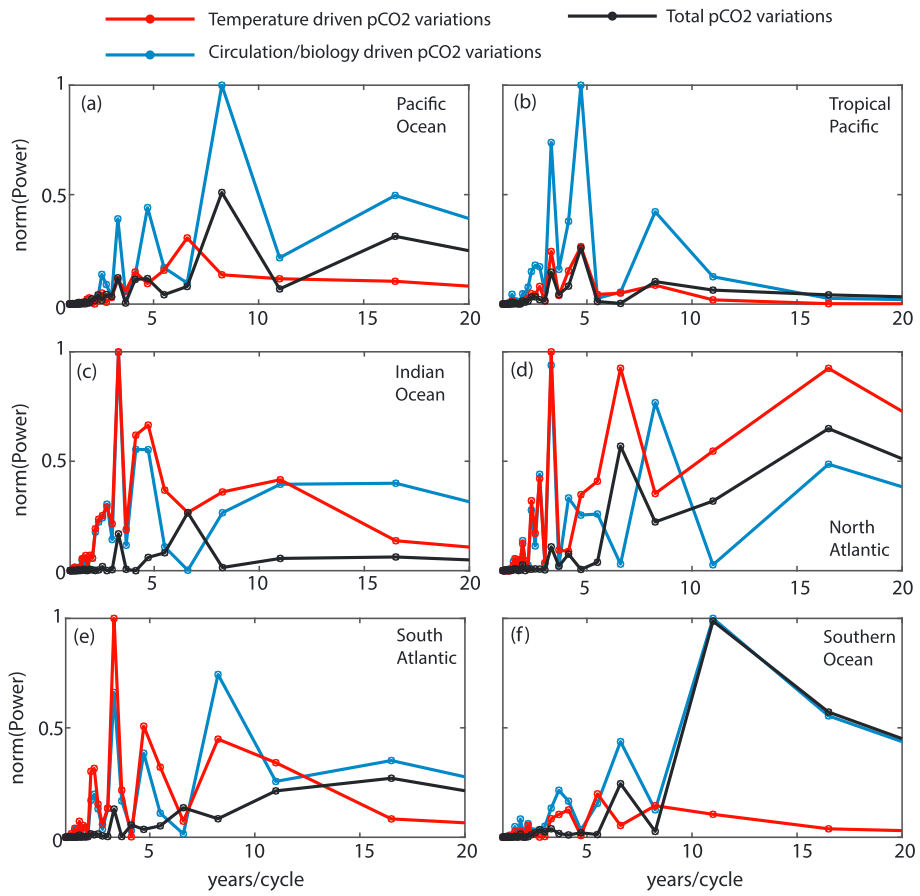

Figure 3. Normalized sea surface pCO_2 anomalies in frequency space (black) in comparison with their thermal (red) and nonthermal (blue) components for the six large-scale ocean regions, namely, (a) the Pacific Ocean excluding the tropics, (b) the Tropical Pacific, (c) the Indian Ocean, (d) the North Atlantic, (e) the South Atlantic, and (f) the Southern Ocean.

respectively), their power spectra show again a much tighter link ($R = 0.83$ and 0.87, respectively). A closer look at the drivers (Figure 3d) reveals that the situation is substantially different between the North and South Atlantic. In the North Atlantic the temperature-driven pCO_2 spectrum (Figure 3d) almost perfectly matches the AMO spectrum (Figure 2b), highlighting the dominant role of the AMO which transitioned to a positive (i.e., warming) phase in the 1990's (McKinley et al., 2011). This suggests that surface ocean temperature variability and the resulting variability in pCO_2 solubility is the main driver in recent North Atlantic pCO_2 variability as suggested by Breeden and McKinley (2016). The nonthermal component only in part compensates the thermally driven pCO_2 variations, but most visually in the low frequency spectrum where the total pCO_2 variability nearly vanishes. The nonthermal component further suggests additional variability at 8-year intervals matching those of the PDO. This suggests a connection in the northern Hemisphere between the Atlantic and Pacific Ocean as suggested by Steinman et al. (2015). In the South Atlantic in contrast (Figure 3e) the dominant low frequency pCO_2 variability results largely from variations in the nonthermal pCO_2 component, whereas almost all high frequency variability vanishes as it is compensated by both components.

An analysis of all pCO_2 power spectra reveals that the Southern Ocean (Figure 2c) shows the smallest amplitude variability on timescales less than a decade. This might be the result of the limited observations here (Bakker et al., 2016; Gruber et al., 2019; Lenton et al., 2013) that prohibit the neural network method from fully reconstructing high frequency variability visible in the SAM spectrum. This has also been shown in Landschützer et al. (2015) where an alternative interpolation method by Rödenbeck et al. (2014) reveals stronger year-to-year variations in the Southern Ocean. Both Southern Ocean pCO_2 and SAM spectra are however the only two that illustrate a maximum between 10 and 15 years. This is in agreement with observed

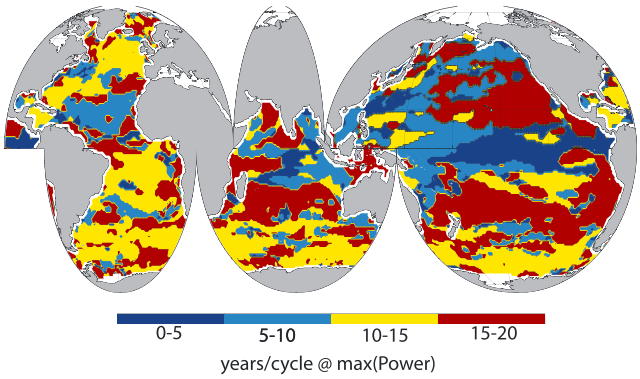

Figure 4. Map highlighting the dominant oscillation period for each 1° × 1° pixel of the global ocean for the observation-based sea surface pCO_2 estimate considering the full 34-year time series.

variations from recent study investigating the CO_2 variability south of Tasmania based on in situ measurements (Xue et al., 2018), whereas a study by Gregor et al. (2018) suggests that modes of summer variability are substantially smaller in the Southern Ocean. While the anomaly time series between the pCO_2 and the SAM index exhibit low correlations ($R = 0.01$), the power spectrum suggests a moderate link ($R = 0.35$) between the two. Previous studies have linked a positive SAM trend to the poleward shift and westerly wind intensification (Fyfe & Saenko, 2006; Le Quéré et al., 2007; Lovenduski et al., 2007), resulting in an increasing upwelling of inorganic carbon, yet it is not resolved if the SAM can explain the observed variations in the Southern Ocean carbon flux (Fay et al., 2014; Landschützer et al., 2015; Ritter et al., 2017). The separation into drivers (Figure 3f) shows that nearly all Southern Ocean variability can be linked to the nonthermal component, which is in agreement with previous studies. However, while basin-wide of lesser importance, Landschützer et al. (2015) have shown that thermal trends can dominate regionally. For example, in the Pacific sector of the Southern Ocean, Landschützer et al. (2015) find that the air-sea CO_2 flux increase in the 2000's is dominated by surface cooling.

The choice of large-scale regions and the building of the average of the pCO_2 anomaly signal might have caused finer scale structures to be averaged out, in particular since regions with different seasonal drivers are combined. Therefore, we repeat our power spectrum analysis for each 1° × 1° pixel of the pCO_2 field. Figure 4 illustrates a map of the dominant cycles, that is, the oscillations with the largest amplitude. While patchy in places the overall structure of this map does reveal some familiar patterns. The analysis shows that the slowest oscillations occur in the subtropics of the Pacific and Indian Oceans, roughly coincident with the ocean gyres, that is, systems where we indeed would expect low frequency variability to dominate. In contrast, the high frequency variability oscillations with a period less than 5 years dominates the Tropical Pacific Ocean in agreement with Feely et al. (2006) and Ishii et al. (2014). As identified in Figure 2c for the whole Southern Ocean also the spatially more refined analysis suggests a dominant oscillation in the order of 10–15 years plausibly linked to the SAM driven wind variations (Fyfe & Saenko, 2006; Le Quéré et al., 2007; Lovenduski et al., 2007). A more surprising image results from the Atlantic Ocean where the spatially refined analysis suggests a dominant oscillation period of 10–15 years over most of the Atlantic Ocean, which is in contrast to the pronounced peak at an oscillation cycle of >15 years in the spectrum of Figure 2 as a result from the spatial average. The local differences in the North Atlantic might result from the regional influence of the North Atlantic Oscillation, which has been shown to be the dominant mode of pCO_2 variability in the subpolar gyre (Metzl et al., 2010; Schuster et al., 2013). Overall our study illustrates that the oscillation periods dominating the pCO_2 variability amplitude are on the order of 10 years and longer and thus, our relatively short observational record can only reconstruct one to two oscillation periods.

4. Conclusions

Our results based on the past record from 1982 through 2015 of the observation-based SOM-FFN sea surface pCO_2 product reveals substantial regional differences in the anomaly time series, with the strongest anomalies in the Tropical Pacific. Unlike the other regions, high frequency variability is absent in the Southern Ocean, which is likely the result of the limited observational coverage. A fast-fourier analysis reveals that there is a significant regional correspondence between the observed variations over the past 34 years and the most commonly used climate indices, suggesting a climate modulated surface ocean pCO_2 and corresponding air-sea CO_2 exchange globally. In general, the correlation between the basin-wide frequency spectra is larger than the correlation of the anomaly time series, indicating that lagged responses and possible teleconnections might mask the direct link between anomalies.

A further decomposition into thermal and nonthermal pCO_2 drivers reveals that while thermal and nonthermal effects largely oppose each other, for most of the ocean the surface ocean pCO_2 variability is driven by changing ocean circulation and/or biology, with the exception of the Indian Ocean and the North Atlantic, where we find a strong correspondence between the AMO and thermally driven pCO_2 variations.

A spatially refined analysis shows that the dominant oscillation patterns follow known oceanic structures such as gyres and current systems, highlighting the regional complexity of the ocean. From 1982 through 2015, we find high spectral power in pCO_2 oscillations at periods of ≥10 years, calling into question whether we can conclude detectability of these oscillations from the rather short time series, particularly since single events, such as forced trends arising from volcanic eruptions might have contributed to this observed variability (see, e.g., C. D. Jones & Cox, 2001). Future work using millennia-long preindustrial control simulations and/or large ensembles of historical simulations from state-of-the-art climate models should investigate whether the observed variability is of internal (e.g., driven by climate) or forced (e.g., volcanic) origin (Lovenduski et al., 2015; McKinley et al., 2016) and help to determine how many years of observation-based pCO_2 time series we would need to faithfully detect climate driven variations in the air-sea CO_2 flux (see, e.g., Lovenduski et al., 2015).

Acknowledgments
P.L. is supported by the Max Planck Society for the advancement of Science. N.S.L. is grateful for funding from the U.S. National Science Foundation (OCE-1752724, OCE-1558225). T.I. received funding from the project CRESCENDO of the European Union's Horizon 2020 research and innovation programme under grant agreement 641816. We thank C. Li and J. Marotzke from the Max Planck Institute for Meteorology in Hamburg for their comments. Results from the neural network-based SOM-FFN method are publicly available online (https://www.nodc.noaa.gov/ocads/oceans/SPCO2_1982_2015_ETH_SOM_FFN.html).

References

Assmann, K. M., Bentsen, M., Segschneider, J., & Heinze, C. (2010). An isopycnic ocean carbon cycle model. *Geoscientific Model Development*, *3*, 143–167.

Aumont, O., & Bopp, L. (2006). Globalizing results from ocean in situ iron fertilization studies. *Global Biogeochemical Cycles*, *20*, GB2017. https://doi.org/10.1029/2005GB002591

Bakker, D. C. E., Pfeil, B., Landa, C. S., Metzl, N., O'Brien, K. M., Olsen, A., et al. (2016). A multi-decade record of high-quality fCO_2 data in version 3 of the Surface Ocean CO_2 Atlas (SOCAT). *Earth System Science Data*, *8*(2), 383–413. https://doi.org/10.5194/essd-8-383-2016

Breeden, M. L., & McKinley, G. A. (2016). Climate impacts on multidecadal pCO_2 variability in the North Atlantic. *Biogeosciences*, *13*, 3387–3396. https://doi.org/10.5194/bg-13-3387-2016

Buitenhuis, E. T., Rivkin, R. B., Sailley, S., & Le Quéré, C. (2010). Biogeochemical fluxes through microzooplankton. *Global Biogeochemical Cycles*, *24*, GB4015. https://doi.org/10.1029/2009GB003601

DeVries, T., Holzer, M., & Primeau, F. (2017). Recent increase in oceanic carbon uptake driven by weaker upper-ocean overturning. *Nature*, *542*, 215–218. https://doi.org/10.1038/nature21068

Deser, C., Phillips, A. S., Tomas, R. A., Okumura, Y. M., Alexander, M., Capotondi, A., et al. (2012). ENSO and Pacific decadal variability in the community climate system model version 4. *Journal of Climate*, *25*, 2622–2651.

Doney, S. C., Lima, I., Feely, R. A., Glover, D. M., Lindsay, K., Mahowald, N., et al. (2009). Mechanisms governing interannual variability in upper-ocean inorganic carbon system and air-sea CO_2 fluxes: Physical climate and atmospheric dust. *Deep-Sea Research II*, *56*, 640–655. https://doi.org/10.1016/j.dsr2.2008.12.006

Enfield, D. B., Mestas-Nunez, A. M., & Trimble, P. J. (2001). The Atlantic multidecadal oscillation and it's relation to rainfall and river flows in the continental U.S. *Geophysical Research Letters*, *28*, 2077–2080.

Fay, A. R., & McKinley, G. A. (2013). Global trends in surface ocean pCO_2 from in situ data. *Global Biogeochemical Cycles*, *27*, 541–557. https://doi.org/10.1002/gbc.20051

Fay, A. R., & McKinley, G. A. (2014). Global ocean biomes: Mean and temporal variability. *Earth System Science Data*, *6*, 273–284. https://doi.org/10.5194/essd-6-273-2014

Fay, A. R., McKinley, G. A., & Lovenduski, N. S. (2014). Southern Ocean carbon trends: Sensitivity to methods. *Geophysical Research Letters*, *41*, 6833–6840. https://doi.org/10.1002/2014GL061324

Feely, R. A., Takahashi, T., Wanninkhof, R., McPhaden, M. J., Cosca, C. E., Sutherland, S. C., & Carr, M.-E. (2006). Decadal variability of the air-sea CO_2 fluxes in the equatorial Pacific Ocean. *Journal of Geophysical Research*, *111*, C08S90. https://doi.org/10.1029/2005JC003129

Feely, R. A., Wanninkhof, R., Takahashi, T., & Tans, P. (1999). Influence of El Niño on the equatorial Pacific contribution to atmospheric CO_2 accumulation. *Nature*, *398*, 597–601. https://doi.org/10.1038/19273

Frölicher, T. L., Sarmiento, J. L., Paynter, D. J., Dunne, J. P., Krasting, J. P., & Winton, M. (2015). Dominance of the southern ocean in anthropogenic carbon and heat uptake in CMIP5 models. *Journal of Climate*, *28*(2), 862–886. https://doi.org/10.1175/JCLI-D-14-00117.1

Fyfe, J. C., & Saenko, O. A. (2006). Simulated changes in extratropical southern hemisphere winds and currents. *Geophysical Research Letters*, *33*, L06701. https://doi.org/10.1029/2005GL025332

Galbraith, E. D., Gnanadesikan, A., Dunne, J. P., & Hiscock, M. R. (2010). Regional impacts of iron-light colimitation in a global biogeochemical model. *Biogeosciences*, *7*, 1043–1064. https://doi.org/10.5194/bg-7-1043-2010

Graven, H. D., Gruber, N., Key, R., Khatiwala, S., & Giraud, X. (2012). Changing controls on oceanic radiocarbon: New insights on shallow-to-deep ocean exchange and anthropogenic CO_2 uptake. *Journal of Geophysical Research*, *117*, C10005. https://doi.org/10.1029/2012JC008074

Gregor, L., Kok, S., & Monteiro, P. M. S. (2018). Interannual drivers of the seasonal cycle of CO_2 in the southern ocean. *Biogeosciences*, *15*(8), 2361–2378. https://doi.org/10.5194/bg-15-2361-2018

Gruber, N., Gloor, M., Mikaloff Fletcher, S. E., Doney, S. C., Dutkiewicz, S., Follows, M. J., et al. (2009). Oceanic sources, sinks, and transport of atmospheric CO_2. *Global Biogeochemical Cycles*, *23*, GB1005. https://doi.org/10.1029/2008GB003349

Gruber, N., Landschützer, P., & Lovenduski, N. S. (2019). The variable Southern Ocean carbon sink. *Annual Review of Marine Science*, *11*(1), 159–186. https://doi.org/10.1146/annurev-marine-121916-063407, pMID: 30212259.

Ilyina, T., Six, K., Segschneider, J., Maier-Reimer, E., Li, H., & Nunez-Riboni, I. (2013). The global ocean biogeochemistry model HAMOOC: Model architecture and performance as component of the MPI-Earth system model in different CMIP5 experimental realizations. *Journal of Advances in Modeling Earth Systems*, *5*, 287–315. https://doi.org/10.1002/jame.20017

Ishii, M., Feely, R. A., Rodgers, K. B., Park, G.-H., Wanninkhof, R., Sasano, D., et al. (2014). Air-sea CO_2 flux in the Pacific Ocean for the period 1990–2009. *Biogeosciences*, *11*(3), 709–734. https://doi.org/10.5194/bg-11-709-2014

Jones, C. D., & Cox, P. M. (2001). Modeling the volcanic signal in the atmospheric CO2 record. *Global Biogeochemical Cycles*, *15*(2), 453–465. https://doi.org/10.1029/2000GB001281

Jones, S. D., Le Quéré, C., Rödenbeck, C., Manning, A. C., & Olsen, A. (2015). A statistical gap-filling method to interpolate global monthly surface ocean carbon dioxide data. *Journal of Advances in Modeling Earth Systems*, *7*, 1554–1575. https://doi.org/10.1002/2014MS000416

Khatiwala, S., Tanhua, T., Mikaloff Fletcher, S., Gerber, M., Doney, S. C., Graven, H. D., et al. (2013). Global ocean storage of anthropogenic carbon. *Biogeosciences*, *10*, 2169–2191. https://doi.org/10.5194/bg-10-2169-2013

Landschützer, P., Gruber, N., & Bakker, D. C. E. (2016). Decadal variations and trends of the global ocean carbon sink. *Global Biogeochemical Cycles*, *30*, 1396–1417. https://doi.org/10.1002/2015GB005359

Landschützer, P., Gruber, N., Bakker, D. C. E., & Schuster, U. (2014). Recent variability of the global ocean carbon sink. *Global Biogeochemical Cycles*, *28*, 927–949. https://doi.org/10.1002/2014GB004853

Landschützer, P., Gruber, N., Bakker, D. C. E., Schuster, U., Nakaoka, S., Payne, M. R., et al. (2013). A neural network-based estimate of the seasonal to inter-annual variability of the Atlantic Ocean carbon sink. *Biogeosciences*, *10*, 7793–7815. https://doi.org/10.5194/bg-10-7793-2013

Landschützer, P., Gruber, N., Bakker, D., Stemmler, I., & Six, K. (2018). Strengthening seasonal marine CO_2 variations due to increasing atmospheric CO_2. *Nature Climate Change*, *8*, 146–150. https://doi.org/10.1038/s41558-017-0057-x

Landschützer, P., Gruber, N., Haumann, F. A., Rödenbeck, C., Bakker, D. C. E., van Heuven, S., et al. (2015). The reinvigoration of the Southern Ocean carbon sink. *Science*, *349*, 1221–1224. https://doi.org/10.1126/science.aab2620

Le Quéré, C., Andrew, R. M., Friedlingstein, P., Sitch, S., Hauck, J., Pongratz, J., et al. (2018). Global carbon budget 2018. *Earth System Science Data*, *10*(4), 2141–2194. https://doi.org/10.5194/essd-10-2141-2018

Le Quéré, C., Orr, J. C., Monfray, P., Aumont, O., & Madec, G. (2000). Interannual variability of the oceanic sink of CO_2 from 1979 through 1997. *Global Biogeochemical Cycles*, *14*(4), 1247–1265. https://doi.org/10.1029/1999GB900049

Le Quéré, C., Rödenbeck, C., Buitenhuis, E. T., Conway, T. J., Langenfelds, R., Gomez, A., et al. (2007). Saturation of the southern ocean CO_2 sink due to recent climate change. *Science*, *316*, 1735–1738. https://doi.org/10.1126/science.1136188

Lefèvre, N., Veleda, D., Araujo, M., & Caniaux, G. (2016). Variability and trends of carbon parameters at a time series in the eastern tropical Atlantic. *Tellus B: Chemical and Physical Meteorology*, *68*(1), 30305. https://doi.org/10.3402/tellusb.v68.30305

Lenton, A., Tilbrook, B., Law, R. M., Bakker, D., Doney, S. C., Gruber, N., et al. (2013). Sea-air CO_2 fluxes in the Southern Ocean for the period 1990-2009. *Biogeosciences*, *10*, 4037–4054. https://doi.org/10.5194/bg-10-4037-2013

Li, H. M., Ilyina, T., Müller, W. A., & Sienz, F. (2016). Decadal predictions of the North Atlantic CO_2 uptake. *Nature Communications*, *7*, 11076.

Lovenduski, N. S., Gruber, N., Doney, S. C., & Lima, D. I. (2007). Enhanced CO_2 outgassing in the Southern Ocean from a positive phase of the southern annular mode. *Global Biogeochemical Cycles*, *21*, GB2026. https://doi.org/10.1029/2006GB002900

Lovenduski, N. S., Long, M. C., & Lindsay, K. (2015). Natural variability in the surface ocean carbonate ion concentration. *Biogeosciences*, *12*, 6321–6335. https://doi.org/10.5194/bg-12-6321-2015

Lovenduski, N. S., Yeager, S. G., Lindsay, K., & Long, M. C. (2019). Predicting near-term variability in ocean carbon uptake. *Earth System Dynamics*, *10*(1), 45–57. https://doi.org/10.5194/esd-10-45-2019

Marshall, G. J. (2003). Trends in the southern annular mode from observations and reanalyses. *Journal of Climate*, *16*, 4134–4143.

Matear, R. J., & Lenton, A. (2008). Impact of historical climate change on the Southern Ocean carbon cycle. *Journal of Climate*, *21*, 5820–5834.

McKinley, G. A., Fay, A. R., Takahashi, T., & Metzl, N. (2011). Convergence of atmospheric and North Atlantic carbon dioxide trends on multidecadal timescales. *Nature Geoscience*, *4*, 606–610. https://doi.org/10.1038/NGEO1193

McKinley, G. A., Follows, M. J., & Marshall, J. (2004). Mechanisms of air-sea CO_2 flux variability in the equatorial Pacific and the North Atlantic. *Global Biogeochemical Cycles*, *18*, GB2011. https://doi.org/10.1029/2003GB002179

McKinley, G. A., Pilcher, D. J., Fay, A. R., Lindsay, K., Long, M. C., & Lovenduski, N. S. (2016). Timescales for detection of trends in the ocean carbon sink. *Nature*, *530*, 469–472. https://doi.org/10.1038/nature16958

Metzl, N., Corbière, A., Reverdin, G., Lenton, A., Takahashi, T., Olsen, A., et al. (2010). Recent acceleration of the sea surface fCO_2 growth rate in the North Atlantic subpolar gyre (1993-2008) revealed by winter observations. *Global Biogeochemical Cycles*, *24*, GB4004. https://doi.org/10.1029/2009gb003658

Nakaoka, S., Telszewski, M., Nojiri, Y., Yasunaka, S., Miyazaki, C., Mukai, H., & Usui, N. (2013). Estimating temporal and spatial variation of ocean surface pCO_2 in the North Pacific using a self-organizing map neural network technique. *Biogeosciences*, *10*, 6093–6106. https://doi.org/10.5194/bg-10-6093-2013

Ritter, R., Landschützer, P., Gruber, N., Fay, A. R., Iida, Y., Jones, S., et al. (2017). Observation-based trends of the Southern Ocean carbon sink. *Geophysical Research Letters*, *44*, 12,339–12,348. https://doi.org/10.1002/2017GL074837

Rödenbeck, C., Bakker, D., Gruber, N., Iida, Y., Jacobson, A. R., Jones, S., et al. (2015). Data-based estimates of the ocean carbon sink variability—First results of the surface ocean pCO_2 mapping intercomparison (SOCOM). *Biogeosciences Discuss*, *12*, 14,049–14,104. https://doi.org/10.5194/bgd-12-14049-2015

Rödenbeck, C., Bakker, D. C. E., Metzl, N., Olsen, A., Sabine, C., Cassar, N., et al. (2014). Interannual sea-air CO_2 flux variability from an observation-driven ocean mixed-layer scheme. *Biogeosciences*, *11*(17), 4599–4613. https://doi.org/10.5194/bg-11-4599-2014

Sabine, C. L., Hankin, S., Koyuk, H., Bakker, D. C., Pfeil, B., Olsen, A., et al. (2013). Surface Ocean CO_2 Atlas (SOCAT) gridded data products. *Earth System Science Data*, *5*, 145–153. https://doi.org/10.5194/essd-5-145-2013

Sarma, V. V. S. S., Lenton, A., Law, R. M., Metzl, N., Patra, P. K., Doney, S., et al. (2013). Sea-air CO_2 fluxes in the Indian Ocean between 1990 and 2009. *Biogeosciences*, *10*(11), 7035–7052. https://doi.org/10.5194/bg-10-7035-2013

Schuster, U., McKinley, G. A., Bates, N., Chevallier, F., Doney, S. C., Fay, A. R., et al. (2013). Atlantic and Arctic sea-air CO_2 fluxes, 1990–2009. *Biogeosciences*, *10*, 607–627. https://doi.org/10.5194/bg-10-607-2013

Schuster, U., & Watson, A. J. (2007). A variable and decreasing sink for atrmospheric CO_2 in the North Atlantic. *Journal of Geophysical Research*, *112*, C11006. https://doi.org/10.1029/2006JC003941

Séférian, R., Berthet, S., & Chevallier, M. (2018). Assessing the decadal predictability of land and ocean carbon uptake. *Geophysical Research Letters*, *45*, 2455–2466. https://doi.org/10.1002/2017GL076092

Steinman, B. A., Mann, M. E., & Miller, S. K. (2015). Atlantic and Pacific multidecadal oscillations and northern hemisphere temperatures. *Science*, *347*, 988. https://doi.org/10.1126/science.1257856

Takahashi, T., Olafsson, J., Goddard, J., Chipman, D., & Sutherland, S. (1993). Seasonal variation of CO_2 and nutrients in the high-latitude surface oceans: A comparative study. *Global Biogeochemical Cycles*, *7*, 843–878. https://doi.org/10.1029/93GB02263

Takahashi, T., Sutherland, S. C., & Kozyr, A. (2018). Global ocean surface water partial pressure of CO_2 database: Measurements performed during 1957–2017 (version 2017) (Tech. rep. ORNL/CDIAC-160, NDP-088(V2017). (NCEI Accession 0160492). Version 4.4): NOAA National Centers for Environmental Information. Dataset.[access date 29-05-2018. https://doi.org/10.3334/CDIAC/OTG.NDP088(V2015)

Takahashi, T., Sutherland, S. C., Sweeney, C., Poisson, A., Metzl, N., Tilbrook, B., et al. (2002). Global sea-air CO_2 flux based on climatological surface ocean pCO_2, and seasonal biological and temperature effects. *Deep-Sea Research II*, *49*, 1601–1622.

Thomas, H., Prowe, F. A. E., Lima, I. D., Doney, S. C., Wanninkhof, R., Greatbatch, R. J., et al. (2008). Changes in the North Atlantic oscillation influence CO_2 uptake in the North Atlantic over the past 2 decades. *Global Biogeochemical Cycles*, *22*, GB4027. https://doi.org/10.1029/2007GB003167

Valsala, V., Maksyutov, S., & Murtugudde, R. (2010). Possible interannual to interdecadal variabilities of the Indonesian through flow water pathways in the Indian Ocean. *Journal of Geophysical Research*, *115*, C10016. https://doi.org/10.1029/2009JC005735

Wolter, K. (1987). The Southern Oscillation in surface circulation and climate over the tropical Atlantic, eastern Pacific, and Indian Oceans as captured by cluster analysis. *Journal of Applied Meteorology and Climatology*, *26*, 540–558.

Wolter, K., & Timlin, M. S. (2011). El Niño/Southern Oscillation behaviour since 1871 as diagnosed in an extended multivariate ENSO index (MEI.ext). *International Journal of Climatology*, *31*, 14.

Xue, L., Cai, W.-J., Takahashi, T., Gao, L., Wanninkhof, R., Wei, M., et al. (2018). Climatic modulation of surface acidification rates through summertime wind forcing in the Southern Ocean. *Nature Communications*, *9*(1), 3240. https://doi.org/10.1038/s41467-018-05443-7

Zeng, J., Nojiri, Y., Landschützer, P., Telszewski, M., & Nakaoka, S. (2014). A global surface ocean f CO_2 climatology based on a feed-forward neural network. *Journal of Atmospheric and Oceanic Technology*, *31*, 1838–1849. https://doi.org/10.1175/JTECH-D-13-00137.1

Zhang, Y., Wallace, J. M., & Battisti, D. S. (1997). ENSO-like interdecadal variability: 1900-93. *Journal of Climate*, *10*, 1004–1020.